

Self-consistent calculations of spectral densities in the $O(N)$ model: improving the Hartree-Fock approximation by including nonzero decay widths

Dirk Röder*

*Institut für Theoretische Physik, Johann Wolfgang Goethe-Universität,
Max von Laue-Str. 1, D-60438 Frankfurt/Main, Germany*

Jörg Ruppert†

Department of Physics, Duke University, Box 90305, Durham, NC 27708, USA

Dirk H. Rischke‡

*Institut für Theoretische Physik and Frankfurt Institute for Advanced Studies,
Johann Wolfgang Goethe-Universität, Max von Laue-Str. 1, D-60438 Frankfurt/Main, Germany*

(Dated: December 17, 2018)

We study the linear sigma model with $O(N)$ symmetry at nonzero temperature in the framework of the Cornwall-Jackiw-Tomboulis formalism. Extending the set of two-particle irreducible diagrams by adding sunset diagrams to the usual Hartree-Fock contributions, we derive a new approximation scheme which extends the standard Hartree-Fock approximation by the inclusion of nonzero decay widths. In this approximation, in-medium modifications of the meson masses as well as decay and collisional broadening effects are self-consistently taken into account. As compared to the standard Hartree-Fock approximation, the temperature for the chiral symmetry restoring phase transition is lowered by $\sim 20 - 25\%$. For large temperatures, the spectral densities of the σ -meson and the pion become degenerate, as required for the chirally symmetric phase.

I. INTRODUCTION

For zero quark masses, the QCD Lagrangian exhibits a global chiral $U(N_f)_r \times U(N_f)_\ell$ or, equivalently, $U(N_f)_V \times U(N_f)_A$ symmetry, where N_f is the number of quark flavors, and $V \equiv r + \ell$, $A \equiv r - \ell$. In the vacuum, the $U(1)_A$ anomaly [1] breaks this symmetry explicitly to $U(N_f)_V \times SU(N_f)_A$. Furthermore, a nonvanishing chiral condensate $\langle \bar{q}q \rangle \sim (300 \text{ MeV})^3$ breaks this symmetry spontaneously to $U(N_f)_V$ [2], leading to $N_f^2 - 1$ pseudoscalar Goldstone bosons which constitute the effective degrees of freedom at low energies. In nature, chiral symmetry is also explicitly broken by nonvanishing quark masses, which accounts for the physical masses of the pions, kaons, etc.

At temperatures of the order of $\sim \langle \bar{q}q \rangle^{1/3}$, the thermal excitation energy is large enough to expect the restoration of chiral symmetry. At such energy scales, the QCD coupling constant is still large, rendering perturbative calculations unreliable. Thus, one has to resort to nonperturbative methods to study chiral symmetry restoration. A first-principle approach is lattice QCD [3]. Lattice QCD calculations have determined the temperature T_c for chiral symmetry restoration to be of order 150 MeV at zero quark chemical potential [4]. These calculations, however, face several technical problems.

The first is that they become numerically very difficult for physically realistic, i.e., small, values of the up- and down-quark masses. Although progress in this direction has been made [5], most studies use unphysically large values. Another problem is that, at nonzero chemical potential, lattice

*Electronic address: roeder@th.physik.uni-frankfurt.de

†Electronic address: ruppert@phy.duke.edu

‡Electronic address: drischke@th.physik.uni-frankfurt.de

QCD calculations are hampered by the fermion sign problem and become increasingly unreliable for chemical potentials larger than (a factor π times) the temperature [6].

An alternative nonperturbative approach to study chiral symmetry restoration is via chiral effective theories. These theories have the same global $U(N_f)_r \times U(N_f)_\ell$ symmetry as QCD but, since quark and gluons are integrated out, do not possess the local $SU(3)_c$ color symmetry of QCD. The effective low-energy degrees of freedom are the (pseudo-) Goldstone bosons of the QCD vacuum, i.e., the pseudoscalar mesons. However, in the chirally symmetric phase these particles become degenerate with their chiral partners, the scalar mesons. Therefore, an appropriate effective theory to study chiral symmetry restoration in QCD is the linear sigma model [7, 8] which treats both scalar and pseudoscalar degrees of freedom on the same footing. The advantage of chiral effective theories over lattice QCD calculations is that their numerical treatment (within some many-body approximation scheme) is comparatively simple and that there is no problem to consider arbitrary quark chemical potential.

At nonzero temperature T , ordinary perturbation theory in terms of the coupling constant g breaks down in the sense that one can no longer order different contributions according to powers of g [9]. This is because the new energy scale introduced by the temperature can conspire with the typical momentum scale p of a process so that gT/p is no longer of order g , but can be of order 1 [10, 11]. Consequently, all terms of order gT/p have to be taken into account which requires the resummation of certain classes of diagrams.

A convenient resummation method is provided by the extension of the Cornwall-Jackiw-Tomboulis (CJT) formalism [12] to nonzero temperatures and chemical potentials. The CJT formalism is equivalent to the Φ -functional approach of Luttinger and Ward [13] and Baym [14]. It generalizes the concept of the effective action $\Gamma[\bar{\phi}]$ for the expectation value $\bar{\phi}$ of the one-point function in the presence of external sources to that for the effective action

$$\Gamma[\bar{\phi}, \bar{G}] = S[\bar{\phi}] + \frac{1}{2} \text{Tr} \ln \bar{G}^{-1} + \frac{1}{2} \text{Tr}(G^{-1} \bar{G} - 1) + \Gamma_2[\bar{\phi}, \bar{G}] \quad (1)$$

for $\bar{\phi}$ and the expectation value \bar{G} of the two-point function in the presence of external sources. Here, $S[\bar{\phi}]$ is the tree-level action, G^{-1} the inverse tree-level two-point function, and $\Gamma_2[\bar{\phi}, \bar{G}]$ the sum of all two-particle irreducible (2PI) vacuum diagrams with internal lines given by \bar{G} . (For an extension of this approach to three- and more-point functions, see [15, 16, 17, 18].) The stationary points of this functional,

$$\left. \frac{\delta \Gamma[\bar{\phi}, \bar{G}]}{\delta \bar{\phi}} \right|_{\bar{\phi}=\varphi, \bar{G}=\mathcal{G}} = 0, \quad \left. \frac{\delta \Gamma[\bar{\phi}, \bar{G}]}{\delta \bar{G}} \right|_{\bar{\phi}=\varphi, \bar{G}=\mathcal{G}} = 0, \quad (2)$$

provide self-consistent equations for the expectation values of the one- and two-point functions $\bar{\phi}$ and \bar{G} in the *absence* of external sources, denoted as φ and \mathcal{G} , respectively. The latter is the Dyson-Schwinger equation,

$$\mathcal{G}^{-1} = G^{-1} + \Pi, \quad (3)$$

where

$$\Pi \equiv -2 \left. \frac{\delta \Gamma_2[\bar{\phi}, \bar{G}]}{\delta \bar{G}} \right|_{\bar{\phi}=\varphi, \bar{G}=\mathcal{G}} \quad (4)$$

is the self-energy. As long as Γ_2 contains *all* 2PI diagrams, the CJT effective action is exact. Of course, it is practically impossible to compute all 2PI diagrams, and one has to truncate Γ_2 , for instance at some order in the number of loops. The advantage of the CJT formalism is that *any* truncation of Γ_2 yields a many-body approximation scheme which preserves the symmetries of the tree-level action, if the expectation values $\bar{\phi}$ and \bar{G} transform as first- and second-rank tensors of these symmetries [14]. The solution of Eqs. (2) is thermodynamically consistent and conserves the

Noether currents. However, Ward-Takahashi identities for higher-order vertex functions may be violated because of the truncation of Γ_2 [19].

The most popular among these many-body approximation schemes is the Hartree-Fock approximation. In this case, Γ_2 solely contains diagrams of so-called “double-bubble” topology, cf. Fig. 1 a–c. Note that, in Refs. [20, 21, 22, 23], this scheme has been termed “Hartree” approximation. However, since the exchange contributions with respect to internal indices are in fact included, it is more appropriate to call it “Hartree-Fock” approximation. Neglecting the exchange contributions leads to the actual Hartree approximation which, in the case of the $O(N)$ model, has also been termed “large- N ” approximation [20, 21]. In the Hartree-Fock approximation, the self-energies, which according to Eq. (4) are obtained by cutting lines in the diagrams for Γ_2 , only consist of “tadpole” diagrams, cf. Figs. 2 b,c, and 3 a,c. For the chiral effective theories, such as the $U(N_f)_r \times U(N_f)_\ell$ and $O(N)$ models, this approximation scheme has been studied in great detail [20, 21, 22, 23, 24, 25, 26, 27]. The Hartree-Fock approximation is a very simple approximation scheme, since tadpole self-energies do not have an imaginary part and, consequently, all particles are stable quasiparticles. Moreover, since tadpoles are independent of energy and momentum, the Dyson-Schwinger equations for the propagators reduce to fix-point equations for the in-medium masses.

There are, however, several problems with the Hartree-Fock approximation related to the truncation of Γ_2 . For instance, in the case of the $O(N)$ model, it does not correctly reproduce the order of the chiral symmetry restoring phase transition and it violates Goldstone’s theorem in the sense that the Goldstone bosons do not remain massless for nonzero temperatures $0 < T < T_c$. Several ways to remedy this shortcoming have been suggested. The simplest one is to neglect subleading contributions in $1/N$, leading to the Hartree (or large- N , see discussion above) approximation [20, 21]. Here, the Goldstone bosons remain massless for $T < T_c$ and the transition is of second order, as expected from universality class arguments [28]. Another possibility to restore Goldstone’s theorem is via so-called “external” propagators [19, 29, 30, 31, 32]. These objects are obtained from the Hartree-Fock propagators by additionally resumming all diagrams pertaining to the Random Phase Approximation (RPA), with internal lines given by the Hartree-Fock propagators. Another way to restore the second-order nature of the chiral phase transition is to include so-called “two-particle point-irreducible” (2PPI) contributions to Γ_2 [33, 34, 35].

In this work, we are not concerned with these formal shortcomings of the Hartree-Fock approximation: we focus exclusively on the case realized in nature where chiral symmetry is already explicitly broken by (small) nonzero quark masses, such that the pion is no longer a Goldstone boson and assumes a mass $M_\pi \simeq 139.5$ MeV in vacuum [36]. Our goal in this work is to include the nonzero decay width of the particles in a self-consistent many-body approximation scheme. To this end, one has to go beyond the Hartree-Fock approximation and add other diagrams to Γ_2 which, upon cutting lines according to Eq. (4), yield self-energies with nonzero imaginary part. The most simple of such diagrams, and the ones considered in the following, are those of the so-called “sunset” topology, cf. Fig. 1 d,e, leading to the self-energy diagrams shown in Figs. 2 d,e and 3 d.

The self-energies arising from the sunset diagrams in Γ_2 depend on the energy and the momentum of the incoming particle. Therefore, the Dyson-Schwinger equations no longer reduce to fix-point equations for the in-medium masses. Since the self-energies now have a nonzero imaginary part, implying a finite lifetime of the corresponding particles, the spectral densities are no longer delta-functions. It is therefore convenient to rewrite the Dyson-Schwinger equations for the propagators into a set of self-consistent integral equations for the spectral densities which has to be solved numerically.

The paper is organized as follows. In Sec. II we discuss the application of the CJT formalism to the $O(N)$ model. In Sec. III we discuss our new approximation scheme which extends the standard Hartree-Fock approximation by including nonzero decay widths. Numerical results for the in-medium masses and decay widths of σ -mesons and pions, as well as their spectral densities are discussed in Sec. IV. Section V concludes this paper with a summary of our results. Technical details are deferred to the appendices.

We denote 4-vectors by capital letters, $X^\mu \equiv (x_0, \mathbf{x})$, with \mathbf{x} being a 3-vector of modulus $x \equiv |\mathbf{x}|$. We use the imaginary-time formalism to compute quantities at nonzero temperature. Integrals over

4-momentum $K^\mu = (k_0, \mathbf{k})$ are denoted as

$$\int_K f(K) \equiv T \sum_{n=-\infty}^{\infty} \int \frac{d^3k}{(2\pi)^3} f(-i\omega_n, \mathbf{k}), \quad (5)$$

where T is the temperature and $\omega_n = 2\pi nT$, $n = 0, \pm 1, \pm 2, \dots$ are the bosonic Matsubara frequencies. Our units are $\hbar = c = k_B = 1$. The metric tensor is $g^{\mu\nu} = \text{diag}(+, -, -, -)$.

II. THE $O(N)$ MODEL IN THE CJT FORMALISM

In this section we discuss the application of the CJT formalism to the $O(N)$ model. In Sec. IV we shall present the numerical results for the case $N = 4$. The Lagrangian of the $O(N)$ linear sigma model is given by

$$\mathcal{L}(\phi) = \frac{1}{2} \partial_\mu \phi \cdot \partial^\mu \phi - U(\phi) \quad (6)$$

where $\phi \equiv (\phi_1, \boldsymbol{\pi})$, with the first component ϕ_1 corresponding to the scalar σ -meson and the other components $\boldsymbol{\pi} = (\phi_2, \dots, \phi_N)$ corresponding to the pseudoscalar pions. The function $U(\phi)$ is the tree-level potential,

$$U(\phi) = \frac{1}{2} \mu^2 \phi \cdot \phi + \frac{\lambda}{N} (\phi \cdot \phi)^2 - H \phi_1. \quad (7)$$

The constant μ^2 is the bare mass and $\lambda > 0$ is the four-point coupling constant. For $\mu^2 < 0$ the $O(N)$ symmetry is spontaneously broken to $O(N-1)$, leading to $N-1$ Goldstone bosons, the pions. The parameter H breaks the symmetry explicitly, giving a mass to the pion. The determination of the parameters μ^2 , λ , and H as functions of the vacuum masses of σ -meson and pion, as well as the pion decay constant, is discussed in detail in Appendix B.

We assume translational invariance so that we may consider the effective potential V instead of the effective action (1). For translationally invariant systems, these two quantities are related via

$$\Gamma[\bar{\sigma}, \bar{\boldsymbol{\pi}}, \bar{S}, \bar{P}] = -\frac{\Omega_3}{T} V[\bar{\sigma}, \bar{\boldsymbol{\pi}}, \bar{S}, \bar{P}], \quad (8)$$

where Ω_3 is the 3-volume of the system, and $\bar{\sigma}, \bar{\boldsymbol{\pi}}, \bar{S}, \bar{P}$ are the expectation values of the one- and two-point functions for the scalar and pseudoscalar fields in the presence of external sources [12]. We are interested in the case where these sources are zero, i.e., in the stationary points of Γ or V , cf. Eq. (2). Because the vacuum of QCD has even parity, the expectation values of the pseudoscalar fields are zero, $\bar{\boldsymbol{\pi}} = 0$, and we shall simply omit the dependence of V on $\bar{\boldsymbol{\pi}}$ in the following.

Then, the effective potential for the $O(N)$ model in the CJT formalism reads [21, 23]

$$\begin{aligned} V[\bar{\sigma}, \bar{S}, \bar{P}] &= U(\bar{\sigma}) + \frac{1}{2} \int_Q [\ln \bar{S}^{-1}(Q) + S^{-1}(Q; \bar{\sigma}) \bar{S}(Q) - 1] \\ &+ \frac{N-1}{2} \int_Q [\ln \bar{P}^{-1}(Q) + P^{-1}(Q; \bar{\sigma}) \bar{P}(Q) - 1] + V_2[\bar{\sigma}, \bar{S}, \bar{P}], \end{aligned} \quad (9)$$

where $U(\bar{\sigma})$ is the tree-level potential (7), evaluated at $\phi = (\bar{\sigma}, 0, \dots, 0)$. The quantities S^{-1} and P^{-1} are the inverse tree-level propagators for scalar and pseudoscalar mesons,

$$S^{-1}(K; \bar{\sigma}) = -K^2 + m_\sigma^2(\bar{\sigma}), \quad (10a)$$

$$P^{-1}(K; \bar{\sigma}) = -K^2 + m_\pi^2(\bar{\sigma}), \quad (10b)$$

where the tree-level masses are

$$m_\sigma^2(\bar{\sigma}) = \mu^2 + \frac{12\lambda}{N} \bar{\sigma}^2, \quad (11a)$$

$$m_\pi^2(\bar{\sigma}) = \mu^2 + \frac{4\lambda}{N} \bar{\sigma}^2. \quad (11b)$$

The functional V_2 in Eq. (9) is related to Γ_2 in Eq. (1) via $\Gamma_2 = -(\Omega_3/T) V_2$. The Hartree-Fock approximation is defined by restricting the sum of all 2PI diagrams, V_2 , to the three double-bubble diagrams shown in Figs. 1 a, b, and c,

$$V_2^a[\bar{P}] \equiv (N+1)(N-1) \frac{\lambda}{N} \left[\int_Q \bar{P}(Q) \right]^2, \quad (12a)$$

$$V_2^b[\bar{S}] \equiv 3 \frac{\lambda}{N} \left[\int_Q \bar{S}(Q) \right]^2, \quad (12b)$$

$$V_2^c[\bar{S}, \bar{P}] \equiv 2(N-1) \frac{\lambda}{N} \int_Q \bar{S}(Q) \int_L \bar{P}(L). \quad (12c)$$

As explained in the introduction, in order to include the nonzero decay width of the particles we have to go beyond the Hartree-Fock approximation by additionally including the sunset diagrams of Figs. 1 d and e. These diagrams have an explicit dependence on $\bar{\sigma}$,

$$V_2^d[\bar{\sigma}, \bar{S}, \bar{P}] \equiv \frac{1}{2} 2(N-1) \left(\frac{4\lambda\bar{\sigma}}{N} \right)^2 \int_L \int_Q \bar{S}(L) \bar{P}(Q) \bar{P}(L+Q), \quad (13a)$$

$$V_2^e[\bar{\sigma}, \bar{S}] \equiv \frac{1}{2} 3! \left(\frac{4\lambda\bar{\sigma}}{N} \right)^2 \int_L \int_Q \bar{S}(L) \bar{S}(Q) \bar{S}(L+Q). \quad (13b)$$

The complete expression for V_2 is obtained by the sum of the contributions (12a) – (13b),

$$V_2 = V_2^a + V_2^b + V_2^c + V_2^d + V_2^e. \quad (14)$$

The expectation values of the one- and two-point functions in the absence of external sources, σ and \mathcal{S} , \mathcal{P} , are determined from the stationary points of V ,

$$\left. \frac{\delta V}{\delta \bar{\sigma}} \right|_{\bar{\sigma}=\sigma, \bar{S}=\mathcal{S}, \bar{P}=\mathcal{P}} = 0, \quad \left. \frac{\delta V}{\delta \bar{S}} \right|_{\bar{\sigma}=\sigma, \bar{S}=\mathcal{S}, \bar{P}=\mathcal{P}} = 0, \quad \left. \frac{\delta V}{\delta \bar{P}} \right|_{\bar{\sigma}=\sigma, \bar{S}=\mathcal{S}, \bar{P}=\mathcal{P}} = 0, \quad (15)$$

leading to an equation for the scalar condensate σ ,

$$H = \mu^2 \sigma + \frac{4\lambda}{N} \sigma^3 + \frac{4\lambda}{N} \sigma \int_Q [3\mathcal{S}(Q) + (N-1)\mathcal{P}(Q)] + \left. \frac{\delta V_2}{\delta \bar{\sigma}} \right|_{\bar{\sigma}=\sigma, \bar{S}=\mathcal{S}, \bar{P}=\mathcal{P}}, \quad (16a)$$

where

$$\left. \frac{\delta V_2}{\delta \bar{\sigma}} \right|_{\bar{\sigma}=\sigma, \bar{S}=\mathcal{S}, \bar{P}=\mathcal{P}} = \left(\frac{4\lambda}{N} \right)^2 \sigma \left[2(N-1) \int_L \int_Q \mathcal{S}(L) \mathcal{P}(Q) \mathcal{P}(L+Q) + 3! \int_L \int_Q \mathcal{S}(L) \mathcal{S}(Q) \mathcal{S}(L+Q) \right], \quad (16b)$$

and to the Dyson-Schwinger equations for the scalar and pseudoscalar propagators,

$$S^{-1}(K; \sigma) = S^{-1}(K; \sigma) + \Sigma[K; \sigma], \quad (16c)$$

$$\mathcal{P}^{-1}(K; \sigma) = \mathcal{P}^{-1}(K; \sigma) + \Pi[K; \sigma]. \quad (16d)$$

Here we introduced the self-energies of the scalar and pseudoscalar fields,

$$\Sigma = \Sigma^a + \Sigma^b + \Sigma^c + \Sigma^d + \Sigma^e, \quad (17a)$$

$$\Pi = \Pi^a + \Pi^b + \Pi^c + \Pi^d + \Pi^e, \quad (17b)$$

with

$$\Sigma^a \equiv 2 \frac{\delta V_2^a}{\delta \bar{S}} \Big|_{\bar{\sigma}=\sigma, \bar{S}=S, \bar{P}=\mathcal{P}} = 0, \quad (18a)$$

$$\Sigma^b \equiv 2 \frac{\delta V_2^b}{\delta \bar{S}} \Big|_{\bar{\sigma}=\sigma, \bar{S}=S, \bar{P}=\mathcal{P}} = \frac{4\lambda}{N} 3 \int_Q \mathcal{S}(Q), \quad (18b)$$

$$\Sigma^c \equiv 2 \frac{\delta V_2^c}{\delta \bar{S}} \Big|_{\bar{\sigma}=\sigma, \bar{S}=S, \bar{P}=\mathcal{P}} = \frac{4\lambda}{N} (N-1) \int_Q \mathcal{P}(Q), \quad (18c)$$

$$\Sigma^d[K; \sigma] \equiv 2 \frac{\delta V_2^d}{\delta \bar{S}} \Big|_{\bar{\sigma}=\sigma, \bar{S}=S, \bar{P}=\mathcal{P}} = \left(\frac{4\lambda\sigma}{N} \right)^2 2(N-1) \int_Q \mathcal{P}(K-Q)\mathcal{P}(Q), \quad (18d)$$

$$\Sigma^e[K; \sigma] \equiv 2 \frac{\delta V_2^e}{\delta \bar{S}} \Big|_{\bar{\sigma}=\sigma, \bar{S}=S, \bar{P}=\mathcal{P}} = \left(\frac{4\lambda\sigma}{N} \right)^2 3 \cdot 3! \int_Q \mathcal{S}(K-Q)\mathcal{S}(Q), \quad (18e)$$

and

$$\Pi^a \equiv \frac{2}{N-1} \frac{\delta V_2^a}{\delta \bar{P}} \Big|_{\bar{\sigma}=\sigma, \bar{S}=S, \bar{P}=\mathcal{P}} = \frac{4\lambda}{N} (N+1) \int_Q \mathcal{P}(Q), \quad (19a)$$

$$\Pi^b \equiv \frac{2}{N-1} \frac{\delta V_2^b}{\delta \bar{P}} \Big|_{\bar{\sigma}=\sigma, \bar{S}=S, \bar{P}=\mathcal{P}} = 0, \quad (19b)$$

$$\Pi^c \equiv \frac{2}{N-1} \frac{\delta V_2^c}{\delta \bar{P}} \Big|_{\bar{\sigma}=\sigma, \bar{S}=S, \bar{P}=\mathcal{P}} = \frac{4\lambda}{N} \int_Q \mathcal{S}(Q), \quad (19c)$$

$$\Pi^d[K; \sigma] \equiv \frac{2}{N-1} \frac{\delta V_2^d}{\delta \bar{P}} \Big|_{\bar{\sigma}=\sigma, \bar{S}=S, \bar{P}=\mathcal{P}} = \left(\frac{4\lambda\sigma}{N} \right)^2 4 \int_Q \mathcal{P}(K-Q)\mathcal{S}(Q), \quad (19d)$$

$$\Pi^e \equiv \frac{2}{N-1} \frac{\delta V_2^e}{\delta \bar{P}} \Big|_{\bar{\sigma}=\sigma, \bar{S}=S, \bar{P}=\mathcal{P}} = 0. \quad (19e)$$

The calculation of the self-energy contributions Eqs. (18) and (19) corresponds to opening internal lines in the diagrams of Fig. 1. Employing this procedure to the double-bubble diagrams leads to the tadpole contributions for the self-energies of the σ -meson (see Figs. 2 b, c) and the pion (see Figs. 3 a, c). This defines the Hartree-Fock approximation. Additionally, the sunset diagrams of Figs. 1 d, e lead to the one-loop contributions shown in Figs. 2 d, e and 3 d. The latter contributions depend on the energy and the momentum of the particles and lead to nonvanishing imaginary parts for the self-energies. The explicit calculation of the self-energies (18) and (19) is discussed in Appendix A.

III. IMPROVING HARTREE-FOCK BY INCLUDING NONZERO DECAY WIDTHS

On the basis of the general framework presented in the preceding section we now discuss in detail how the Hartree-Fock approximation can be improved by including the nonzero decay width of the particles.

As explained in the introduction, we rewrite the set of Dyson-Schwinger equations (16c) and (16d) in terms of a set of integral equations for the spectral densities. In general, the spectral densities for the σ -meson and the pion are defined as

$$\rho_\sigma(\omega, \mathbf{k}) \equiv 2 \text{Im} \mathcal{S}(\omega + i\eta, \mathbf{k}; \sigma), \quad (20a)$$

$$\rho_\pi(\omega, \mathbf{k}) \equiv 2 \text{Im} \mathcal{P}(\omega + i\eta, \mathbf{k}; \sigma). \quad (20b)$$

If the imaginary parts of the self-energies are zero, as in the Hartree-Fock approximation, all particles are stable quasiparticles, i.e., their spectral densities become delta-functions with support on the quasiparticle mass shell,

$$\rho_\sigma(\omega, \mathbf{k}) = 2\pi Z_\sigma[\omega_\sigma(\mathbf{k}), \mathbf{k}] \{ \delta[\omega - \omega_\sigma(\mathbf{k})] - \delta[\omega + \omega_\sigma(\mathbf{k})] \} , \quad (21a)$$

$$\rho_\pi(\omega, \mathbf{k}) = 2\pi Z_\pi[\omega_\pi(\mathbf{k}), \mathbf{k}] \{ \delta[\omega - \omega_\pi(\mathbf{k})] - \delta[\omega + \omega_\pi(\mathbf{k})] \} , \quad (21b)$$

where $\omega_{\sigma,\pi}(\mathbf{k})$ are the quasiparticle energies for σ -mesons and pions, defined by the positive solutions of

$$\omega_\sigma^2(\mathbf{k}) = k^2 + m_\sigma^2(\sigma) + \text{Re} \Sigma[\omega_\sigma(\mathbf{k}), \mathbf{k}; \sigma] , \quad (22a)$$

$$\omega_\pi^2(\mathbf{k}) = k^2 + m_\pi^2(\sigma) + \text{Re} \Pi[\omega_\pi(\mathbf{k}), \mathbf{k}; \sigma] , \quad (22b)$$

and

$$Z_\sigma[\omega_\sigma(\mathbf{k}), \mathbf{k}] \equiv \left| \frac{\partial \mathcal{S}^{-1}(K; \sigma)}{\partial k_0} \right|_{k_0=\omega_\sigma(\mathbf{k})}^{-1} , \quad (23a)$$

$$Z_\pi[\omega_\pi(\mathbf{k}), \mathbf{k}] \equiv \left| \frac{\partial \mathcal{P}^{-1}(K; \sigma)}{\partial k_0} \right|_{k_0=\omega_\pi(\mathbf{k})}^{-1} , \quad (23b)$$

are the wave-function renormalization factors on the quasi-particle mass shell. Since the real parts of the self-energies are even functions of energy, these factors are also even in $\omega_{\sigma,\pi}(\mathbf{k})$. In the Hartree-Fock approximation, the (real parts of the) self-energies do not depend on K^μ , such that

$$\omega_\sigma(k) = \sqrt{k^2 + M_\sigma^2(\sigma)} , \quad \omega_\pi(k) = \sqrt{k^2 + M_\pi^2(\sigma)} , \quad (24)$$

where

$$M_\sigma^2(\sigma) \equiv m_\sigma^2(\sigma) + \text{Re} \Sigma(\sigma) , \quad M_\pi^2(\sigma) \equiv m_\pi^2(\sigma) + \text{Re} \Pi(\sigma) , \quad (25)$$

are the effective σ -meson and pion masses, and

$$Z_\sigma[\omega_\sigma(k)] = \frac{1}{2\omega_\sigma(k)} , \quad Z_\pi[\omega_\pi(k)] = \frac{1}{2\omega_\pi(k)} . \quad (26)$$

For nonvanishing imaginary parts of the self-energies the spectral densities assume the following form:

$$\rho_\sigma(\omega, \mathbf{k}) = - \frac{2 \text{Im} \Sigma(\omega, \mathbf{k}; \sigma)}{[\omega^2 - k^2 - m_\sigma^2(\sigma) - \text{Re} \Sigma(\omega, \mathbf{k}; \sigma)]^2 + [\text{Im} \Sigma(\omega, \mathbf{k}; \sigma)]^2} , \quad (27a)$$

$$\rho_\pi(\omega, \mathbf{k}) = - \frac{2 \text{Im} \Pi(\omega, \mathbf{k}; \sigma)}{[\omega^2 - k^2 - m_\pi^2(\sigma) - \text{Re} \Pi(\omega, \mathbf{k}; \sigma)]^2 + [\text{Im} \Pi(\omega, \mathbf{k}; \sigma)]^2} . \quad (27b)$$

The general calculation of the imaginary parts of the self-energies is discussed in the second part of Appendix A. It turns out that they do not depend on the direction of 3-momentum \mathbf{k} , but only on the modulus k . The tadpole diagrams of Figs. 2 b, c (for the σ -meson) and Figs. 3 a, c (for the

pion) do not have an imaginary part. Thus [see Appendix A, Eq. (A19)],

$$\begin{aligned}
\text{Im } \Sigma(\omega, k; \sigma) &= \text{Im } \Sigma^d(\omega, k; \sigma) + \text{Im } \Sigma^e(\omega, k; \sigma) \\
&= \left(\frac{4\lambda\sigma}{N} \right)^2 \frac{1}{2(2\pi)^3} \frac{1}{k} \int_{-\infty}^{\infty} d\omega_1 d\omega_2 [1 + f(\omega_1) + f(\omega_2)] \delta(\omega - \omega_1 - \omega_2) \\
&\quad \times \int_0^{\infty} dq_1 q_1 dq_2 q_2 \Theta(|q_1 - q_2| \leq k \leq q_1 + q_2) \\
&\quad \times [2(N-1) \rho_\pi(\omega_1, q_1) \rho_\pi(\omega_2, q_2) + 3 \cdot 3! \rho_\sigma(\omega_1, q_1) \rho_\sigma(\omega_2, q_2)] , \tag{28a}
\end{aligned}$$

$$\begin{aligned}
\text{Im } \Pi(\omega, k; \sigma) &= \text{Im } \Pi^d(\omega, k; \sigma) \\
&= \left(\frac{4\lambda\sigma}{N} \right)^2 \frac{1}{2(2\pi)^3} \frac{1}{k} \int_{-\infty}^{\infty} d\omega_1 d\omega_2 [1 + f(\omega_1) + f(\omega_2)] \delta(\omega - \omega_1 - \omega_2) \\
&\quad \times \int_0^{\infty} dq_1 q_1 dq_2 q_2 \Theta(|q_1 - q_2| \leq k \leq q_1 + q_2) \\
&\quad \times 4 \rho_\sigma(\omega_1, q_1) \rho_\pi(\omega_2, q_2) , \tag{28b}
\end{aligned}$$

where $f(\omega) = [\exp(\omega/T) - 1]^{-1}$ is the Bose-Einstein distribution function. These expressions are not ultraviolet divergent and thus do not need to be renormalized.

For the real parts, we employ the following approximation. We only take into account the Hartree-Fock contributions, arising from the tadpole diagrams Figs. 2 b, c (for the σ -meson) and Figs. 3 a, c (for the pion). As discussed above, these contributions do not depend on energy and momentum. The real parts of the diagrams in Figs. 2 d, e and 3 d are functions of energy and momentum and are much harder to compute, involving an additional numerical integration as compared to the respective imaginary parts (28). This has been done in the Hartree (or large- N) approximation to the $O(N)$ linear sigma model in Ref. [37]. In this approximation, the only energy-momentum dependent contribution arises from the diagram in Fig. 2 d. It was found in Ref. [37] that this contribution leads to minor quantitative, but not qualitative, changes of the spectral density of the σ -meson. Therefore, in the present first step where we focus exclusively on the effects of a nonzero decay width, we neglect the real parts of the diagrams in Figs. 2 d, e and 3 d. Consequently [see Appendix A, Eq. (A8)],

$$\begin{aligned}
\text{Re } \Sigma(\sigma) &= \text{Re } \Sigma^b(\sigma) + \text{Re } \Sigma^c(\sigma) \\
&= \frac{4\lambda}{N} \frac{2}{(2\pi)^3} \int_0^{\infty} d\omega dq q^2 [1 + 2f(\omega)] [3 \rho_\sigma(\omega, q) + (N-1) \rho_\pi(\omega, q)] , \tag{29a}
\end{aligned}$$

$$\begin{aligned}
\text{Re } \Pi(\sigma) &= \text{Re } \Pi^a(\sigma) + \text{Re } \Pi^c(\sigma) \\
&= \frac{4\lambda}{N} \frac{2}{(2\pi)^3} \int_0^{\infty} d\omega dq q^2 [1 + 2f(\omega)] [\rho_\sigma(\omega, q) + (N+1) \rho_\pi(\omega, q)] . \tag{29b}
\end{aligned}$$

Since the real parts do not depend on energy and momentum, they only modify the masses of the σ -meson and the pion, cf. Eq. (25). The thermal parts of the self-energies in Eqs. (29), $\sim f(\omega)$ are ultraviolet finite, but the vacuum parts, ~ 1 , are ultraviolet divergent and have to be renormalized. The $O(N)$ linear sigma model is an effective theory which is not valid above a certain energy or momentum scale. Therefore, we choose a particularly simple renormalization scheme, regulating the ultraviolet divergent part of the ω integral in Eqs. (29) by introducing a cut-off Λ , cf. Appendix A. In principle, we could also have chosen to regulate the q integral. However, the spectral density relates the energy to the momentum integral in Eqs. (29). For large momenta q , the spectral density is of appreciable magnitude only in a range of energies $\omega \sim q$, cf. Figs. 6 and 7. Of course, our results will depend on the cut-off Λ ; this dependence will be discussed in Sec. IV. The cut-off prescription is also used to compute the tadpole and the sunset contributions in Eq. (16a) for the condensate, cf. Appendix A. For a more formal treatment of renormalization within the CJT formalism, see for instance Refs. [19, 30, 31].

After obtaining real and imaginary parts (29) and (28), respectively, one inserts them in the expressions (21) (if the imaginary part is zero) or (27) (if the imaginary part is nonzero) for the spectral densities. These spectral densities can then be used to again evaluate the real and imaginary parts of the self-energies. This defines an iterative scheme to self-consistently solve for the spectral densities as functions of energy and momentum. A convenient starting point for this scheme is the Hartree-Fock approximation, i.e., neglecting the imaginary parts altogether.

The self-consistently computed spectral densities obey a sum rule [38],

$$\int_{-\infty}^{\infty} \frac{d\omega}{2\pi} \omega \rho_{\sigma,\pi}(\omega, \mathbf{k}) = 1 . \quad (30)$$

In our calculation, there are two reasons why this sum rule may be violated. One is because we neglected the real parts of the self-energy diagrams in Figs. 2 d, e and 3 d. (The results of Ref. [37] suggest, though, that this has minor impact on the sum rule.) The other is due to the numerical realization of the above described iterative scheme. Numerically, one has to solve for the spectral density on a finite, discretized grid in energy-momentum space. If the imaginary part of the self-energy becomes very small, the spectral density converges towards a delta function. The support of the delta function may be located between grid sites, which causes a loss of spectral strength, which in turn violates the sum rule.

Our prescription to restore the validity of the sum rule is the following. We first check whether the imaginary part is smaller than the grid spacing (in our calculations, 10 MeV in both energy and momentum direction) at the location of the quasiparticle mass shell, $\omega = \omega_{\sigma,\pi}(k)$. If this is the case, we add a sufficiently wide numerical realization of the delta function, δ_{num} , to the original spectral density, $\rho(\omega, k) \rightarrow \rho(\omega, k) + c \cdot \delta_{\text{num}}[\omega - \omega_{\sigma,\pi}(k)]$, where c is a constant that is adjusted so that the sum rule is fulfilled on our energy-momentum grid,

$$\int_{-\omega_{\text{max}}}^{\omega_{\text{max}}} \frac{d\omega}{2\pi} \omega \rho_{\sigma,\pi}(\omega, \mathbf{k}) = 1 , \quad (31)$$

where ω_{max} is the maximum energy on the energy-momentum grid.

On the other hand, if the imaginary part turns out to be sufficiently large, we presume that a possible violation of the sum rule (31) arises from neglecting the real parts of the self-energy diagrams in Figs. 2 d, e and 3 d. In this case, we multiply the spectral density by a constant, $\rho \rightarrow c' \cdot \rho$, where c' is adjusted so that the sum rule (31) is fulfilled. (By comparing the results to the case $c' = 1$, we found that this somewhat *ad hoc* correction procedure does not lead to major quantitative changes, in agreement with the results of Ref. [37].)

Restricting the sum rule to a finite range in energy as in Eq. (31), however, causes the following problem. If the decay width of the particles is very large and consequently the spectral density a rather broad distribution around the quasiparticle mass shell, there will be parts which lie outside the energy-momentum grid. We could estimate the magnitude of this physical effect if we knew the behavior of the spectral density at energies $\omega > \omega_{\text{max}}$. This is possible at zero temperature (with the help of Weinberg's sum rules), but not at nonzero temperature. Here, we simply assume that this effect is sufficiently small to be neglected, i.e., we assume that a possible violation of the sum rule (31) is due to the two above mentioned artifacts and accordingly perform the correction of the spectral density.

Another physical effect which causes a loss of spectral strength is if the quasiparticle energy $\omega_{\sigma,\pi}(k) > \omega_{\text{max}}$. In this case, we do not perform the correction of the spectral density as described above. This occurs at large momenta k , close to the edge of the energy-momentum grid. We checked that, in the numerical calculation of the integrals in Eqs. (28), the integrands become sufficiently small in this region, so that the imaginary parts are not sensitive to this effect.

This concludes the discussion of our improvement of the Hartree-Fock approximation by self-consistently including nonzero decay widths.

IV. RESULTS

In this section we present the numerical results for the $O(4)$ linear sigma model obtained in the Hartree-Fock approximation improved by including nonzero decay widths, as discussed in Sec. III.

The first step is to determine the parameters of the model. This is discussed in detail in Appendix B. The zero-temperature values for the mass of the pion and the scalar condensate are $M_\pi = 139.5$ MeV and $\sigma \equiv f_\pi = 92.4$ MeV [36]. The σ -meson has a large decay width because of its decay into two pions. We take $M_\sigma = 600$ MeV and determine the width self-consistently within our improved Hartree-Fock approximation. For the cut-off required to renormalize the ultraviolet-divergent contributions of loop integrals, we consider two choices, $\Lambda = 0$ and 200 MeV. (As discussed in Appendix B, it is not possible to consider arbitrarily large values for Λ ; for $M_\sigma = 600$ MeV the maximum value is $\Lambda_{\max} = 260$ MeV.) For $\Lambda = 0$, we obtain for the parameters of the $O(4)$ model the values $H = (121.60 \text{ MeV})^3$, $\lambda = 19.943$, and $\mu^2 = -(388.34 \text{ MeV})^2$, while for $\Lambda = 200$ MeV, we have $H = (107.16 \text{ MeV})^3$, $\lambda = 20.303$, and $\mu^2 = -(411.38 \text{ MeV})^2$.

The condensate σ is shown in the left part of Fig. 4 as a function of temperature for the standard and the improved Hartree-Fock approximation. The qualitative behavior is similar in the two approximations: the condensate drops significantly with temperature indicating the restoration of chiral symmetry. Since we consider the case of explicit $O(4)$ symmetry breaking by taking $H \neq 0$ in Eq. (7), the chiral phase transition is a cross-over transition. Nevertheless, one can define a transition temperature, T_χ , as the temperature where the chiral susceptibility $\partial\sigma/\partial T$ assumes a maximum. Quantitatively, the inclusion of a nonzero decay width lowers T_χ as compared to the standard Hartree-Fock approximation by about 20% for $\Lambda = 0$, and by about 25% for $\Lambda = 200$ MeV, respectively. The transition temperature $T_\chi \simeq 160 - 175$ MeV agrees well with recent lattice results, $T_\chi \simeq 172 \pm 5$ MeV for the two-flavor case [4]. (Note, however, that the latter value is extracted from an extrapolation to the chiral limit, while our result is for the case of explicit symmetry breaking, i.e., for nonzero quark masses.)

For the solution of the condensate equation (16a) the relative magnitude of the contribution from the sunset diagrams, Eq. (16b), is negligibly small, of order $\sim 10^{-4}$, and thus can be safely neglected. In turn, not having to compute the integrals pertaining to the double loop, cf. Eq. (A24), considerably speeds up the computation.

In the right part of Fig. 4, we show the effective masses $M_\sigma \equiv \sqrt{m_\sigma^2 + \text{Re}\Sigma}$ and $M_\pi \equiv \sqrt{m_\pi^2 + \text{Re}\Pi}$ of the σ -meson and the pion as functions of temperature in both approximation schemes. Since the decay width of the pion remains comparatively small, cf. Fig. 5, the mass of the pion does not change appreciably when taking the nonzero decay width into account. On the other hand, the large decay width of the σ -meson at temperatures below T_χ , cf. Fig. 5, does influence the mass: in this range of temperatures the mass exhibits a stronger decrease with temperature in the improved Hartree-Fock approximation. At large temperatures $T > T_\chi$, the decay width of the σ -meson becomes negligibly small, cf. Fig. 5, and the mass approaches the value computed in the standard Hartree-Fock approximation. Both σ -meson and pion masses approach each other above T_χ , indicating the restoration of chiral symmetry.

In Fig. 5 we show the decay widths of σ -mesons and pions, defined as [38, 39]

$$\Gamma_\sigma(k) \equiv \frac{\text{Im}\Sigma[\omega_\sigma(k), k; \sigma]}{\omega_\sigma(k)}, \quad \Gamma_\pi(k) \equiv \frac{\text{Im}\Pi[\omega_\pi(k), k; \sigma]}{\omega_\pi(k)}, \quad (32)$$

where $\omega_{\sigma,\pi}(k)$ is the energy on the quasi-particle mass shell, cf. Eq. (22). At small temperatures, due to the possible decay of a σ -meson into two pions, the decay width of the former is large, of the order of its mass. Note that the values of Γ_σ obtained here at $T = 0$ are completely determined by the parameters m^2 , λ , and H of the $O(4)$ model, i.e., without adjusting any additional parameter. They are reasonably close to the experimentally measured value $\Gamma_\sigma \sim 600 - 1000$ MeV [36]. The σ decay width increases with temperature up to a maximum at a temperature $T \simeq 100$ MeV and then decreases rapidly. The decay width of the pion vanishes at $T = 0$. It increases at nonzero temperature and assumes a maximum around $T \simeq 150$ MeV. At this temperature the decay width is

about half of the corresponding pion mass. It decreases rapidly at higher temperature. Although the decay widths of both particles decrease at high temperatures, they do not become degenerate, the decay width of the σ -meson remains about a factor of 8 larger than that of the pion. This difference can be traced to the symmetry factors multiplying the one-loop self-energies for the σ -meson and pion, cf. Eqs. (28). For the σ -meson, there is a factor $2(N-1)$ in front of the pion loop and a factor $3 \cdot 3!$ in front of the σ -loop, so that the overall factor is $\sim 2(N-1) + 3 \cdot 3! = 24$. For the pion, there is only a mixed σ -pion loop with a symmetry factor 4. From this simple argument one already expects that the decay width of the σ -meson is about a factor of 6 larger than that of the pion. The remaining difference comes from the fact that the self-consistently computed spectral densities of σ -meson and pion under the integrals in Eqs. (28) are also different, cf. Fig. 8.

One might argue that, at asymptotically large temperatures, effects from chiral symmetry breaking can no longer play a role and the decay widths, as well as the spectral densities, of σ -meson and pion should become degenerate. This is true in the chiral limit, where there is a thermodynamic phase transition between the phases of broken and restored chiral symmetry, and where $\sigma \equiv 0$ in the latter phase. Here, however, we consider the case of explicitly broken chiral symmetry, where $\sigma > 0$, even when the temperature is very large. Since the decay widths are proportional to σ^2 , they also do not vanish at large temperature. The difference in the symmetry factors for the self-energies of σ -mesons and pions then leads to different values for the decay widths and spectral densities.

The self-consistently calculated spectral densities of the σ -meson and the pion as functions of the external energy ω and momentum k are shown in Fig. 6 and Fig. 7 for different temperatures, $T = 80, 160, 240,$ and 320 MeV. Here we restrict ourselves to the case $\Lambda = 0$; the results for the case $\Lambda = 200$ MeV are quantitatively rather similar. For a detailed discussion, let us fix the momentum at $k = 325$ MeV and consider the spectral densities as functions of energy ω for different temperatures, cf. Fig. 8.

At all temperatures, the pion spectral density (dotted line) exhibits a pronounced peak on the mass shell, at $\omega_\pi(k) = \sqrt{k^2 + M_\pi^2(\sigma)}$. When the temperature is below 200 MeV, such that $M_\pi \simeq 139.5$ MeV, cf. Fig. 4, the peak is located at $\omega_\pi(325 \text{ MeV}) \simeq 350$ MeV. Above $T \sim 200$ MeV, M_π increases significantly with temperature, and the position of the peak shifts towards larger energies, $\omega_\pi(325 \text{ MeV}) \simeq 500$ MeV. The broadening of the peak is due to scattering of the pion off σ -mesons in the medium.

In contrast to the pion spectral density, for temperatures below ~ 170 MeV the σ spectral density (full line) does not exhibit a peak at the mass shell, $\omega_\sigma(k) = \sqrt{k^2 + M_\sigma^2(\sigma)}$. The reason is that $\omega_\sigma(k)$ is still sufficiently large to allow for the decay into two pions. Consequently, in this temperature range the σ spectral density is very broad. On the other hand, for temperatures above ~ 170 MeV, where $\omega_\sigma(k)$ drops below $2 M_\pi$, the two-pion decay channel is closed and the σ spectral density develops a distinct peak, whose width is due to scattering of the σ -mesons off pions and other σ -mesons in the medium.

Two other features of the spectral densities shown in Fig. 8 are noteworthy. The first is the region below the light-cone, $K^2 = \omega^2 - k^2 < 0$, where the mesons are Landau-damped. The second is the two-particle decay threshold. For $\sigma \rightarrow \pi\pi$, this threshold is located at $\omega \sim 2 M_\pi$, for $\sigma \rightarrow \sigma\sigma$, it is at $\omega \sim 2 M_\sigma$, and for $\pi \rightarrow \sigma\pi$ at $\omega \sim M_\sigma + M_\pi$. The threshold is most clearly seen at large temperatures, e.g. $T = 320$ MeV, when both particles become degenerate in mass, $M_\sigma \simeq M_\pi \sim 400$ MeV, and the threshold is at $\omega \sim 900$ MeV.

V. CONCLUSIONS

In this paper we have studied the $O(N)$ linear sigma model at nonzero temperature within a self-consistent many-body resummation scheme. This scheme extends the standard Hartree-Fock approximation by including nonzero decay widths of the particles. In the Hartree-Fock approximation, the self-energies of the particles consist of tadpole diagrams which have no imaginary part. Consequently, all particles are stable quasi-particles. In order to obtain a nonzero decay width, one has to include diagrams in the self-energy, which have a nonzero imaginary part corresponding to

decay and, in a medium, scattering processes.

In order to incorporate the nonzero decay width in a self-consistent way, we apply the Cornwall-Jackiw-Tomboulis formalism. The standard Hartree-Fock approximation is obtained by considering only double-bubble diagrams in the 2PI effective action, leading to the (energy- and momentum-independent) tadpole contributions in the 1PI self-energies. In order to extend the Hartree-Fock approximation, we additionally take into account diagrams of sunset topology in the 2PI effective action. This has the consequence that the 1PI self-energies obtain additional energy- and momentum-dependent one-loop contributions which have a nonzero imaginary part. The spectral densities of σ -mesons and pions are then computed as solutions of a self-consistent set of Dyson-Schwinger equations for the σ -meson and pion two-point functions, coupled to a fix-point equation for the chiral condensate. We only take into account the imaginary parts of the new one-loop contributions. We made sure that the spectral densities obey a standard sum rule by adjusting their normalization, if necessary.

We found that the temperature T_χ for chiral symmetry restoration is about 20 – 25% smaller as compared to the Hartree-Fock approximation when including nonzero particle decay widths. Our value for the temperature of chiral symmetry restoration T_χ agrees reasonably well with lattice results [4]. We computed the decay widths of σ -mesons and pions as a function of temperature. The vacuum value for the σ decay width comes out to be in the experimentally observed range, without adjusting a parameter of the model. It stays approximately constant up to temperatures $\sim T_\chi$ and then decreases sharply with temperature. The pion decay width grows from zero at $T = 0$ to a value ~ 100 MeV at $T \sim T_\chi$, and then also decreases with temperature.

We also investigated the spectral densities of σ -mesons and pions as functions of energy and momentum for temperatures in the range of $T = 80$ to 320 MeV. Below the chiral phase transition, the spectral density of the σ -meson is broad, due to the possible decay into two pions. It develops a peak at the quasi-particle mass shell above the chiral phase transition, when this decay channel is closed. On the other hand, the spectral density of the pion always exhibits a distinct peak at the quasi-particle mass shell. The width of this peak is due to scattering off σ -mesons in the medium. Above the chiral phase transition, the spectral densities of σ -mesons and pions become degenerate in shape.

The present study can be continued along several lines. An important task is to include also the real parts of the self-energy contributions from the sunset diagrams. It would also be of interest to study the chiral limit, in order to see how the sunset diagrams affect the order of the chiral phase transition. In the Hartree-Fock approximation, the chiral phase transition turns out to be of first order, while universality arguments predict it to be of second order.

Other possible future projects are the inclusion of other degrees of freedom, for instance strange scalar and pseudoscalar mesons, baryons [40], and vector mesons [41, 42, 43]. The latter is of particular importance, since in-medium changes in the spectral properties of vector mesons are reflected in the dilepton spectrum [44] which, in turn, is experimentally observable in heavy-ion collisions at GSI-SIS, CERN-SPS and BNL-RHIC energies.

Acknowledgments

J.R. acknowledges support by the Alexander von Humboldt foundation as a Feodor-Lynen fellow. We thank the Center of Scientific Computing of the University of Frankfurt for computational support.

APPENDIX A: THE CALCULATION OF THE DIAGRAMS

In this Appendix we discuss the calculation of the three types of diagrams (see Fig. 9) contributing to the self-energies and the condensate equation. To evaluate them explicitly, we use standard techniques of thermal field theory, see for example Refs. [38, 45, 46].

1. The tadpole diagram

In the following we discuss the calculation of the tadpole diagram in Fig. 9 a as a functional of the spectral density. In the imaginary-time formalism it is given by

$$\mathcal{T} \equiv T \sum_n \int \frac{d^3q}{(2\pi)^3} \Delta(-i\omega_n, \mathbf{q}), \quad (\text{A1})$$

where T is the temperature, and Δ is either the σ -meson or pion propagator.

The first step is to perform the sum over the Matsubara frequencies. To this aim we introduce the mixed representation of the propagator

$$\Delta(-i\omega_n, \mathbf{q}) = \int_0^{1/T} d\tau \exp(-i\omega_n\tau) \Delta(\tau, \mathbf{q}), \quad (\text{A2})$$

with

$$\Delta(\tau, \mathbf{q}) = \int_{-\infty}^{\infty} \frac{d\omega}{2\pi} [\Theta(\tau) + f(\omega)] \rho(\omega, \mathbf{q}) \exp(-\omega\tau), \quad (\text{A3})$$

where $f(\omega) = [\exp(\omega/T) - 1]^{-1}$ is the Bose-Einstein distribution function. With the identity

$$T \sum_n \exp(-i\omega_n\tau) = \sum_{m=-\infty}^{\infty} \delta\left(\tau - \frac{m}{T}\right), \quad (\text{A4})$$

the Matsubara sum can be performed analytically

$$\begin{aligned} \mathcal{T} &= T \sum_n \int \frac{d^3q}{(2\pi)^3} \int_0^{1/T} d\tau \exp(-i\omega_n\tau) \Delta(\tau, \mathbf{q}) \\ &= \int \frac{d^3q}{(2\pi)^3} \int_0^{1/T} d\tau \Delta(\tau, \mathbf{q}) \left[\delta(\tau) + \delta\left(\tau - \frac{1}{T}\right) \right] \\ &= \int \frac{d^3q}{(2\pi)^3} \frac{1}{2} \left[\Delta(0, \mathbf{q}) + \Delta\left(\frac{1}{T}, \mathbf{q}\right) \right] \\ &= \int \frac{d^3q}{(2\pi)^3} \Delta(0, \mathbf{q}), \end{aligned} \quad (\text{A5})$$

where use has been made of the KMS condition $\Delta(\tau, \mathbf{q}) \equiv \Delta(\tau - 1/T, \mathbf{q})$. With Eq. (A3) we finally have

$$\mathcal{T} = \int_{-\infty}^{\infty} \frac{d\omega}{2\pi} \int \frac{d^3q}{(2\pi)^3} \left[\frac{1}{2} + f(\omega) \right] \rho(\omega, \mathbf{q}). \quad (\text{A6})$$

Due to isotropy of space, the spectral density of a scalar particle cannot depend on the direction of \mathbf{q} , thus the angular integration can be carried out:

$$\mathcal{T} = 4\pi \int_{-\infty}^{\infty} \frac{d\omega}{2\pi} \int_0^{\infty} \frac{dq}{(2\pi)^3} q^2 \left[\frac{1}{2} + f(\omega) \right] \rho(\omega, q). \quad (\text{A7})$$

Using the fact that the spectral density for bosonic degrees of freedom is an odd function of the energy, $\rho(\omega) = -\rho(-\omega)$,

$$\begin{aligned} \mathcal{T} &= 4\pi \int_0^{\infty} \frac{d\omega}{2\pi} \frac{dq}{(2\pi)^3} q^2 [f(\omega) - f(-\omega)] \rho(\omega, q) \\ &= 4\pi \int_0^{\infty} \frac{d\omega}{2\pi} \frac{dq}{(2\pi)^3} q^2 [1 + 2f(\omega)] \rho(\omega, q). \end{aligned} \quad (\text{A8})$$

This integral can be split into an ultraviolet-finite temperature-dependent part,

$$\mathcal{T}^T = 4\pi \int_0^\infty \frac{d\omega}{2\pi} \frac{dq}{(2\pi)^3} q^2 2f(\omega) \rho(\omega, q) , \quad (\text{A9})$$

and an ultraviolet-divergent vacuum part, which is renormalized by introducing a cut-off Λ for the ω integral,

$$\mathcal{T}^\Lambda = 4\pi \int_0^\infty \frac{d\omega}{2\pi} \frac{dq}{(2\pi)^3} q^2 \Theta(\Lambda - \omega) \rho(\omega, q) , \quad (\text{A10})$$

where $\mathcal{T} \equiv \mathcal{T}^T + \mathcal{T}^\Lambda$.

2. The cut sunset diagram

In this section we calculate the imaginary part of the cut sunset diagram of Fig. 9 b. In the imaginary-time formalism the cut sunset diagram is given by

$$\mathcal{C}(-i\omega_m, \mathbf{k}) \equiv \int_Q \Delta_1(K - Q) \Delta_2(Q) = T \sum_n \int \frac{d^3q}{(2\pi)^3} \Delta_1(-i(\omega_m - \omega_n), \mathbf{k} - \mathbf{q}) \Delta_2(-i\omega_n, \mathbf{q}) \quad (\text{A11})$$

where Δ_1, Δ_2 are the propagators of σ -mesons and/or pions. The major difference between the tadpole diagram, discussed in the last section, and this diagram is that it explicitly depends on the external four-momentum, $K^\mu \equiv (-i\omega_m, \mathbf{k})$.

Analogously to the last section one introduces the mixed representation [see Eq. (A2)] of the propagators Δ_1 and Δ_2

$$\begin{aligned} \mathcal{C}(-i\omega_m, \mathbf{k}) &= T \sum_n \int \frac{d^3q}{(2\pi)^3} \int_0^{1/T} d\tau_1 \exp[-i(\omega_m - \omega_n)\tau_1] \Delta_1(\tau_1, \mathbf{k} - \mathbf{q}) \\ &\quad \times \int_0^{1/T} d\tau_2 \exp(-i\omega_n\tau_2) \Delta_2(\tau_2, \mathbf{q}) . \end{aligned} \quad (\text{A12})$$

The summation over the Matsubara frequencies leads to a delta function [cf. Eq. (A4)]

$$\mathcal{C}(-i\omega_m, \mathbf{k}) = \int \frac{d^3q}{(2\pi)^3} \int_0^{1/T} d\tau \exp(-i\omega_m\tau) \Delta_1(\tau, \mathbf{k} - \mathbf{q}) \Delta_2(\tau, \mathbf{q}) . \quad (\text{A13})$$

Introduction of the spectral densities [see Eq. (A3)] for both propagators in the mixed representation leads to

$$\begin{aligned} \mathcal{C}(-i\omega_m, \mathbf{k}) &= \int \frac{d^3q}{(2\pi)^3} \int_0^{1/T} d\tau \exp(-i\omega_m\tau) \int_{-\infty}^{\infty} \frac{d\omega_1}{2\pi} [1 + f(\omega_1)] \rho_1(\omega_1, \mathbf{k} - \mathbf{q}) \exp(-\omega_1\tau) \\ &\quad \times \int_{-\infty}^{\infty} \frac{d\omega_2}{2\pi} [1 + f(\omega_2)] \rho_2(\omega_2, \mathbf{q}) \exp(-\omega_2\tau) . \end{aligned} \quad (\text{A14})$$

The integration over τ can be performed analytically. Employing the identity

$$\left[\exp\left(-\frac{\omega_1 + \omega_2}{T}\right) - 1 \right] [1 + f(\omega_1)][1 + f(\omega_2)] = -1 - f(\omega_1) - f(\omega_2) , \quad (\text{A15})$$

the expression can be rewritten as

$$\mathcal{C}(-i\omega_m, \mathbf{k}) = \int_{-\infty}^{\infty} \frac{d\omega_1}{2\pi} \frac{d\omega_2}{2\pi} \frac{1 + f(\omega_1) + f(\omega_2)}{i\omega_m + \omega_1 + \omega_2} \int \frac{d^3q}{(2\pi)^3} \rho_1(\omega_1, \mathbf{k} - \mathbf{q}) \rho_2(\omega_2, \mathbf{q}) . \quad (\text{A16})$$

Using the fact that the spectral densities do not depend on the direction of momentum and

$$\int \frac{d^3x}{(2\pi)^3} f(|\mathbf{y} - \mathbf{x}|) g(x) = \frac{2\pi}{y} \frac{1}{(2\pi)^3} \int_0^\infty dx_1 x_1 dx_2 x_2 f(x_1) g(x_2) \times \Theta(|x_1 - x_2| \leq y \leq x_1 + x_2) , \quad (\text{A17})$$

one can perform one angular integration, yielding

$$\begin{aligned} \mathcal{C}(-i\omega_m, \mathbf{k}) &= \int_{-\infty}^\infty \frac{d\omega_1}{2\pi} \frac{d\omega_2}{2\pi} \frac{1 + f(\omega_1) + f(\omega_2)}{i\omega_m + \omega_1 + \omega_2} \\ &\times \frac{2\pi}{k} \frac{1}{(2\pi)^3} \int_0^\infty dq_1 q_1 dq_2 q_2 \rho_1(\omega_1, q_1) \rho_2(\omega_2, q_2) \\ &\times \Theta(|q_1 - q_2| \leq k \leq q_1 + q_2) . \end{aligned} \quad (\text{A18})$$

The imaginary part of the retarded cut sunset diagram can be extracted using analytical continuation, $-i\omega_m \rightarrow \omega + i\epsilon$, and the Dirac identity $\text{Im}1/(x + i\epsilon) = -\pi\delta(x)$,

$$\begin{aligned} \text{Im} \mathcal{C}(\omega, \mathbf{k}) &= \frac{1}{2(2\pi)^3} \frac{1}{k} \int_{-\infty}^\infty d\omega_1 d\omega_2 [1 + f(\omega_1) + f(\omega_2)] \delta(\omega - \omega_1 - \omega_2) \\ &\times \int_0^\infty dq_1 q_1 dq_2 q_2 \Theta(|q_1 - q_2| \leq k \leq q_1 + q_2) \rho_1(\omega_1, q_1) \rho_2(\omega_2, q_2) . \end{aligned} \quad (\text{A19})$$

This integral is finite and therefore does not require renormalization.

3. The sunset diagram

In the imaginary-time formalism the sunset diagram shown in Fig. 9 c is given by the following expression:

$$\mathcal{S} = T^2 \sum_{n,m} \int \frac{d^3l}{(2\pi)^3} \frac{d^3q}{(2\pi)^3} \Delta_1(-i\omega_m, \mathbf{l}) \Delta_2(-i\omega_n, \mathbf{q}) \Delta_3(-i(-\omega_n - \omega_m), -\mathbf{q} - \mathbf{l}) . \quad (\text{A20})$$

We introduce the mixed representation, see Eq. (A2), for the three propagators Δ_1, Δ_2 , and Δ_3 . One can perform the Matsubara sums employing Eq. (A4). In the mixed representation one introduces the spectral densities ρ_1, ρ_2 , and ρ_3 in order to perform the τ integration analytically. Employing the identity

$$\begin{aligned} &\left[\exp\left(-\frac{\omega_1 + \omega_2 + \omega_3}{T}\right) - 1 \right] [1 + f(\omega_1)] [1 + f(\omega_2)] [1 + f(\omega_3)] \\ &= -1 - f(\omega_1) - f(\omega_2) - f(\omega_3) - f(\omega_1)f(\omega_2) - f(\omega_1)f(\omega_3) - f(\omega_2)f(\omega_3) , \end{aligned} \quad (\text{A21})$$

for the Bose-Einstein distribution functions we obtain

$$\begin{aligned} \mathcal{S} &= \int_{-\infty}^\infty \frac{d\omega_1}{2\pi} \frac{d\omega_2}{2\pi} \frac{d\omega_3}{2\pi} \frac{1 + f(\omega_1) + f(\omega_2) + f(\omega_3) + f(\omega_1)f(\omega_2) + f(\omega_1)f(\omega_3) + f(\omega_2)f(\omega_3)}{\omega_1 + \omega_2 + \omega_3} \\ &\times \int \frac{d^3l}{(2\pi)^3} \frac{d^3q}{(2\pi)^3} \rho_1(\omega_1, \mathbf{l}) \rho_2(\omega_2, \mathbf{q}) \rho_3(\omega_3, -\mathbf{q} - \mathbf{l}) . \end{aligned} \quad (\text{A22})$$

Using the fact that the spectral densities do not depend on the direction of momentum, the angular integrals can be carried out with the result

$$\begin{aligned} \mathcal{S} &= \frac{2}{(2\pi)^7} \int_{-\infty}^\infty d\omega_1 d\omega_2 d\omega_3 \int_0^\infty dq_1 q_1 dq_2 q_2 dq_3 q_3 \Theta(|q_1 - q_2| \leq q_3 \leq q_1 + q_2) \\ &\times \frac{1 + f(\omega_1) + f(\omega_2) + f(\omega_3) + f(\omega_1)f(\omega_2) + f(\omega_1)f(\omega_3) + f(\omega_2)f(\omega_3)}{\omega_1 + \omega_2 + \omega_3} \\ &\times \rho_1(\omega_1, q_1) \rho_2(\omega_2, q_2) \rho_3(\omega_3, q_3) . \end{aligned} \quad (\text{A23})$$

Using the antisymmetry of the spectral densities and relabelling integration variables, we finally arrive at

$$\begin{aligned}
\mathcal{S} &= \frac{4}{(2\pi)^7} \int_0^\infty d\omega_1 d\omega_2 d\omega_3 dq_1 q_1 dq_2 q_2 dq_3 q_3 \Theta(|q_1 - q_2| \leq q_3 \leq q_1 + q_2) \\
&\times \left[\frac{f(\omega_1)f(\omega_2) + f(\omega_1)f(\omega_3) + f(\omega_3)f(\omega_2) + f(\omega_1) + f(\omega_2) + f(\omega_3) + 1}{\omega_1 + \omega_2 + \omega_3} \right. \\
&\quad + \frac{f(\omega_1)f(\omega_3) - f(\omega_1)f(\omega_2) + f(\omega_2)f(\omega_3) + f(\omega_3)}{\omega_1 + \omega_2 - \omega_3} \\
&\quad + \frac{f(\omega_1)f(\omega_2) - f(\omega_1)f(\omega_3) + f(\omega_2)f(\omega_3) + f(\omega_2)}{\omega_1 - \omega_2 + \omega_3} \\
&\quad \left. + \frac{f(\omega_1)f(\omega_2) + f(\omega_1)f(\omega_3) - f(\omega_2)f(\omega_3) + f(\omega_1)}{-\omega_1 + \omega_2 + \omega_3} \right] \\
&\times \rho_1(\omega_1, q_1) \rho_2(\omega_2, q_2) \rho_3(\omega_3, q_3) .
\end{aligned} \tag{A24}$$

This integral can be split in an ultraviolet-finite temperature-dependent part,

$$\begin{aligned}
\mathcal{S}^T &= \frac{4}{(2\pi)^7} \int_0^\infty d\omega_1 d\omega_2 d\omega_3 dq_1 q_1 dq_2 q_2 dq_3 q_3 \Theta(|q_1 - q_2| \leq q_3 \leq q_1 + q_2) \\
&\times \left[\frac{f(\omega_1)f(\omega_2) + f(\omega_1)f(\omega_3) + f(\omega_3)f(\omega_2)}{\omega_1 + \omega_2 + \omega_3} \right. \\
&\quad + \frac{f(\omega_1)f(\omega_3) - f(\omega_1)f(\omega_2) + f(\omega_2)f(\omega_3)}{\omega_1 + \omega_2 - \omega_3} \\
&\quad + \frac{f(\omega_1)f(\omega_2) - f(\omega_1)f(\omega_3) + f(\omega_2)f(\omega_3)}{\omega_1 - \omega_2 + \omega_3} \\
&\quad \left. + \frac{f(\omega_1)f(\omega_2) + f(\omega_1)f(\omega_3) - f(\omega_2)f(\omega_3)}{-\omega_1 + \omega_2 + \omega_3} \right] \\
&\times \rho_1(\omega_1, q_1) \rho_2(\omega_2, q_2) \rho_3(\omega_3, q_3) ,
\end{aligned} \tag{A25}$$

an ultraviolet-divergent temperature-dependent part, which is renormalized by introducing a cut-off Λ for one of the ω_i integrals,

$$\begin{aligned}
\mathcal{S}^\Lambda &= \frac{4}{(2\pi)^7} \int_0^\infty d\omega_1 d\omega_2 d\omega_3 dq_1 q_1 dq_2 q_2 dq_3 q_3 \Theta(|q_1 - q_2| \leq q_3 \leq q_1 + q_2) \\
&\times \left[\frac{f(\omega_1)\Theta(\Lambda - \omega_2) + f(\omega_2)\Theta(\Lambda - \omega_1) + f(\omega_3)\Theta(\Lambda - \omega_1)}{\omega_1 + \omega_2 + \omega_3} \right. \\
&\quad \left. + \frac{f(\omega_3)\Theta(\Lambda - \omega_1)}{\omega_1 + \omega_2 - \omega_3} + \frac{f(\omega_2)\Theta(\Lambda - \omega_1)}{\omega_1 - \omega_2 + \omega_3} + \frac{f(\omega_1)\Theta(\Lambda - \omega_2)}{-\omega_1 + \omega_2 + \omega_3} \right] \\
&\times \rho_1(\omega_1, q_1) \rho_2(\omega_2, q_2) \rho_3(\omega_3, q_3) ,
\end{aligned} \tag{A26}$$

and an ultraviolet-divergent vacuum part, which is renormalized by introducing a cut-off Λ for two of the ω_i integrals,

$$\begin{aligned}
\mathcal{S}^{\Lambda\Lambda} &= \frac{4}{(2\pi)^7} \int_0^\infty d\omega_1 d\omega_2 d\omega_3 dq_1 q_1 dq_2 q_2 dq_3 q_3 \Theta(|q_1 - q_2| \leq q_3 \leq q_1 + q_2) \\
&\times \frac{\Theta(\Lambda - \omega_1)\Theta(\Lambda - \omega_2)}{\omega_1 + \omega_2 + \omega_3} \rho_1(\omega_1, q_1) \rho_2(\omega_2, q_2) \rho_3(\omega_3, q_3) ,
\end{aligned} \tag{A27}$$

where $\mathcal{S} \equiv \mathcal{S}^T + \mathcal{S}^\Lambda + \mathcal{S}^{\Lambda\Lambda}$.

APPENDIX B: THE RENORMALIZED PARAMETERS

In this appendix, we discuss how to determine the parameters μ^2 , λ , and H of the $O(N)$ model. At $T = 0$, the equations for the σ -meson and the pion mass are, cf. Eq. (25),

$$M_\sigma^2 = \mu^2 + \frac{4\lambda}{N} [3f_\pi^2 + 3\mathcal{T}_\sigma^\Lambda + (N-1)\mathcal{T}_\pi^\Lambda], \quad (\text{B1a})$$

$$M_\pi^2 = \mu^2 + \frac{4\lambda}{N} [f_\pi^2 + \mathcal{T}_\sigma^\Lambda + (N+1)\mathcal{T}_\pi^\Lambda], \quad (\text{B1b})$$

where the zero-temperature contributions of the tadpole diagrams, $\mathcal{T}_{\sigma,\pi}^\Lambda$, are defined in Eq. (A10). Solving these equations for λ and μ^2 one obtains

$$\lambda \equiv \lambda(\Lambda) = \frac{N}{8} \frac{M_\sigma^2 - M_\pi^2}{f_\pi^2 + \mathcal{T}_\sigma^\Lambda - \mathcal{T}_\pi^\Lambda}, \quad (\text{B2a})$$

$$\mu^2 = -\frac{M_\sigma^2 - 3M_\pi^2}{2} - \frac{4\lambda}{N} (N+2)\mathcal{T}_\pi^\Lambda. \quad (\text{B2b})$$

Equation (16a) for the zero-temperature condensate, $\sigma \equiv f_\pi$, can be written as

$$H = f_\pi \left\{ M_\sigma^2 - \frac{8\lambda f_\pi^2}{N} + \left(\frac{4\lambda}{N} \right)^2 [2(N-1)\mathcal{S}_{\sigma\sigma\sigma}^{\Lambda\Lambda} + 3!\mathcal{S}_{\sigma\pi\pi}^{\Lambda\Lambda}] \right\}, \quad (\text{B2c})$$

where $\mathcal{S}_{\sigma\pi\pi}^{\Lambda\Lambda}$ is the zero-temperature contribution of the sunset diagram consisting of two pions and one σ -meson, and $\mathcal{S}_{\sigma\sigma\sigma}^{\Lambda\Lambda}$ is the corresponding one consisting of three σ -mesons, respectively. These quantities are defined in Eq. (A27). Since these contributions are small, we neglect them.

The term $\sim H$ in the tree-level potential breaks the residual $O(N-1)$ symmetry of the vacuum explicitly and favors a certain value for the scalar condensate $\sigma \equiv f_\pi$. The sign of this value is determined by the sign of H . For $H > 0$, we must have $\sigma > 0$. In order to preserve this relation, we read off from Eq. (B2c) that λ is restricted from above by $N M_\sigma^2 / (8f_\pi^2)$. From Eq. (B2a), this constraint leads to a restriction on the possible values of the cut-off Λ . For a given mass of the σ -meson, the maximum value for the cut-off, Λ_{max} , decreases with increasing M_σ . For instance, for $M_\sigma = 400, 600, 800$ MeV, one obtains $\Lambda_{\text{max}} = 340, 260, 220$ MeV, respectively. A similar behavior for the σ -meson mass as function of the cut-off has been discussed in Ref. [47].

-
- [1] G. 't Hooft, Phys. Rept. **142**, 357 (1986).
 - [2] C. Vafa and E. Witten, Nucl. Phys. **B234**, 173 (1984).
 - [3] F. Karsch, Lect. Notes Phys. **583**, 209 (2002), hep-lat/0106019.
 - [4] E. Laermann and O. Philipsen, Ann. Rev. Nucl. Part. Sci. **53**, 163 (2003), hep-ph/0303042.
 - [5] Z. Fodor and S. D. Katz, JHEP **04**, 050 (2004), hep-lat/0402006.
 - [6] P. de Forcrand and O. Philipsen, Nucl. Phys. **B642**, 290 (2002), hep-lat/0205016.
 - [7] M. Levy, Nuovo Cim. **52**, 23 (1967).
 - [8] M. Gell-Mann and M. Levy, Nuovo Cim. **16**, 705 (1960).
 - [9] L. Dolan and R. Jackiw, Phys. Rev. **D9**, 3320 (1974).
 - [10] E. Braaten and R. D. Pisarski, Phys. Rev. Lett. **64**, 1338 (1990).
 - [11] E. Braaten and R. D. Pisarski, Nucl. Phys. **B337**, 569 (1990).
 - [12] J. M. Cornwall, R. Jackiw, and E. Tomboulis, Phys. Rev. **D10**, 2428 (1974).
 - [13] J. M. Luttinger and J. C. Ward, Phys. Rev. **118**, 1417 (1960).
 - [14] G. Baym, Phys. Rev. **127**, 1391 (1962).
 - [15] R. E. Norton and J. M. Cornwall, Ann. Phys. **91**, 106 (1975).
 - [16] H. Kleinert, Fortsch. Phys. **30**, 187 (1982).
 - [17] M. E. Carrington, Eur. Phys. J. **C35**, 383 (2004), hep-ph/0401123.

- [18] J. Berges, Phys. Rev. **D70**, 105010 (2004), hep-ph/0401172.
- [19] H. van Hees and J. Knoll, Phys. Rev. **D66**, 025028 (2002), hep-ph/0203008.
- [20] N. Petropoulos, J. Phys. **G25**, 2225 (1999), hep-ph/9807331.
- [21] J. T. Lenaghan and D. H. Rischke, J. Phys. **G26**, 431 (2000), nucl-th/9901049.
- [22] J. T. Lenaghan, D. H. Rischke, and J. Schaffner-Bielich, Phys. Rev. **D62**, 085008 (2000), nucl-th/0004006.
- [23] D. Röder, J. Ruppert, and D. H. Rischke, Phys. Rev. **D68**, 016003 (2003), nucl-th/0301085.
- [24] G. Baym and G. Grinstein, Phys. Rev. **D15**, 2897 (1977).
- [25] A. Bochkarev and J. I. Kapusta, Phys. Rev. **D54**, 4066 (1996), hep-ph/9602405.
- [26] H.-S. Roh and T. Matsui, Eur. Phys. J. **A1**, 205 (1998), nucl-th/9611050.
- [27] G. Amelino-Camelia, Phys. Lett. **B407**, 268 (1997), hep-ph/9702403.
- [28] R. D. Pisarski and F. Wilczek, Phys. Rev. **D29**, 338 (1984).
- [29] Z. Aouissat, O. Bohr, and J. Wambach, Mod. Phys. Lett. **A13**, 1827 (1998), hep-ph/9710419.
- [30] H. van Hees and J. Knoll, Phys. Rev. **D65**, 025010 (2002), hep-ph/0107200.
- [31] H. Van Hees and J. Knoll, Phys. Rev. **D65**, 105005 (2002), hep-ph/0111193.
- [32] G. Aarts, D. Ahrensmeier, R. Baier, J. Berges, and J. Serreau, Phys. Rev. **D66**, 045008 (2002), hep-ph/0201308.
- [33] H. Vershelde and M. Coppens, Phys. Lett. **B287**, 133 (1992).
- [34] H. Vershelde, Phys. Lett. **B497**, 165 (2001), hep-th/0009123.
- [35] J. Baacke and S. Michalski, Phys. Rev. **D67**, 085006 (2003), hep-ph/0210060.
- [36] S. Eidelman, K. Hayes, K. Olive, M. Aguilar-Benitez, C. Amsler, D. Asner, K. Babu, R. Barnett, J. Beringer, P. Burchat, et al., Physics Letters B **592**, 1+ (2004), URL <http://pdg.lbl.gov>.
- [37] D. Röder (2005), hep-ph/0509232.
- [38] M. Le Bellac, *Thermal Field Theory* (Cambridge University Press, 2000).
- [39] H. A. Weldon, Phys. Rev. **D28**, 2007 (1983).
- [40] C. Beckmann, S. Wilms, and D. H. Rischke, (in preparation).
- [41] H. van Hees and J. Knoll, Nucl. Phys. **A683**, 369 (2000), hep-ph/0007070.
- [42] J. Ruppert and T. Renk, Phys. Rev. **C71**, 064903 (2005), nucl-th/0412047.
- [43] S. Strüber and D. H. Rischke, (in preparation).
- [44] R. Rapp and J. Wambach, Adv. Nucl. Phys. **25**, 1 (2000), hep-ph/9909229.
- [45] A. Das, *Finite Temperature Field Theory* (World Scientific, 1997).
- [46] J. I. Kapusta, *Finite Temperature Field Theory* (Cambridge University Press, 1993).
- [47] F. Cooper, Y. Kluger, E. Mottola, and J. P. Paz, Phys. Rev. **D51**, 2377 (1995), hep-ph/9404357.

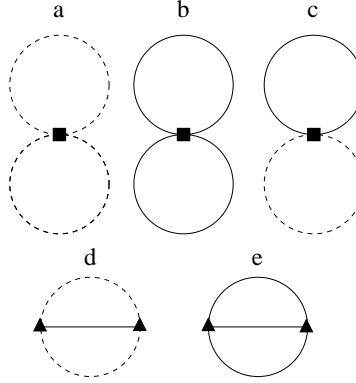


FIG. 1: The set of two-particle irreducible diagrams defining the improved Hartree-Fock approximation for the $O(N)$ model, see Eq. (9). The diagrams a, b, and c are the double-bubble diagrams, and d and e are the sunset diagrams. A full line denotes the full propagator for the σ -meson and a dashed line the full propagator for the pion. The four-particle vertex $\sim \lambda$ is represented by a square and the three-particle vertex $\sim \lambda\sigma$ by a triangle.

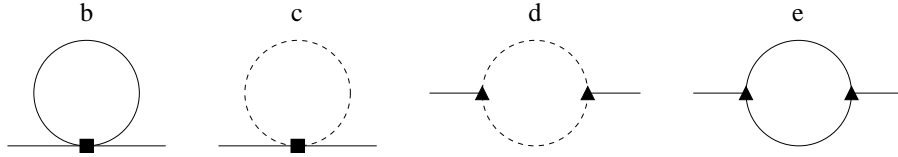


FIG. 2: The self-energy of the σ -meson. The diagrams b and c are tadpole contributions generated by cutting an internal σ -line in the double-bubble diagrams b and c in Fig. 1. The diagrams d and e are one-loop contributions generated by cutting an internal σ -meson line in the sunset diagrams d and e of Fig. 1. Lines and vertices as in Fig. 1.

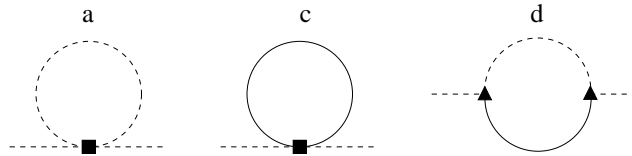


FIG. 3: The self-energy of the pion. The diagrams a and c are tadpole contributions generated by cutting an internal pion line in the double-bubble diagrams a and c in Fig. 1. The diagram d is the one-loop contribution generated by cutting an internal pion line in the sunset diagram d in Fig. 1. Lines and vertices as in Fig. 1.

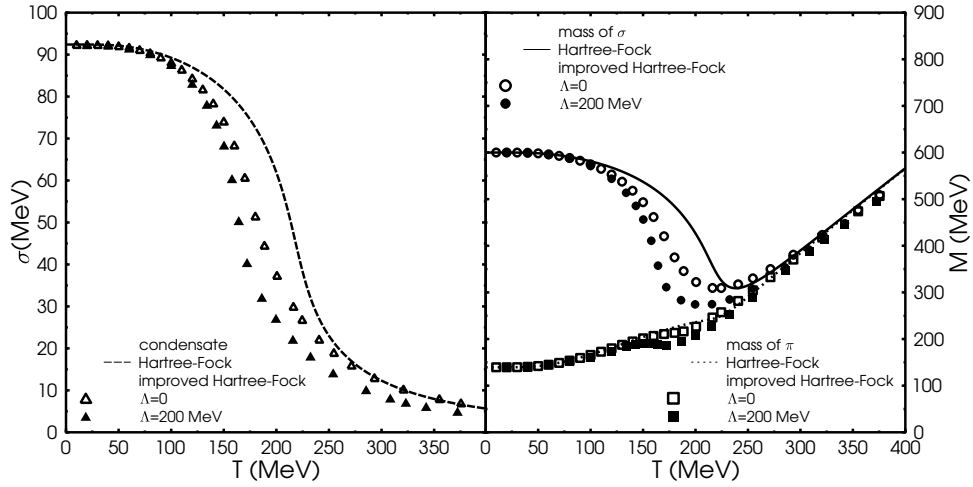


FIG. 4: The values for the condensate (left panel) and the effective masses of the σ -meson and the pion, (right panel) as functions of temperature. The values are calculated in the Hartree-Fock approximation (dashed and solid lines) and in the improved Hartree-Fock approximation (symbols) as discussed in Sec. III.

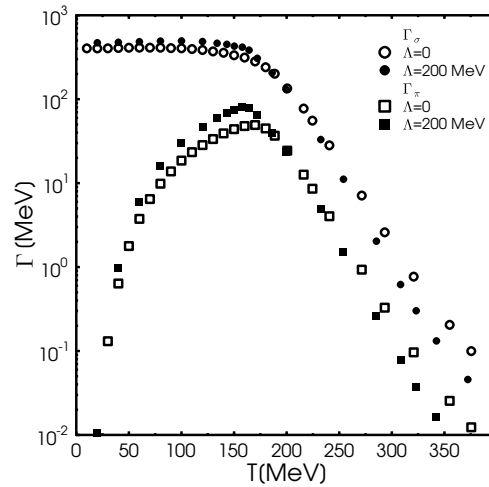


FIG. 5: The decay width of the σ -meson, $\Gamma_\sigma = \text{Im}\Sigma(\omega)/\omega$, and the pion, $\Gamma_\pi = \text{Im}\Pi(\omega)/\omega$, in the improved Hartree-Fock approximation as a function of the temperature at momentum $k = 325$ MeV.

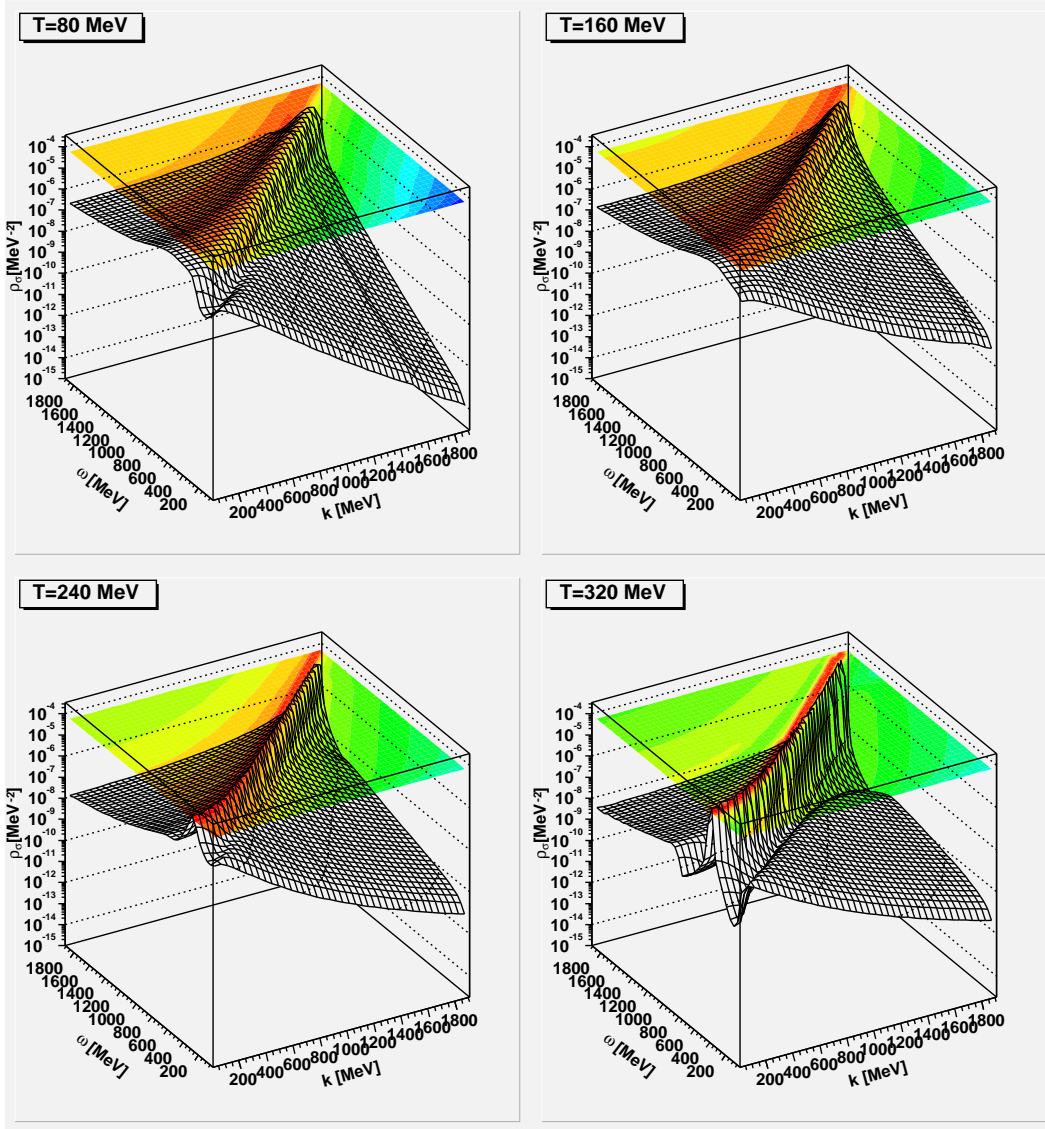


FIG. 6: The spectral density of the σ -meson as a function of energy ω and momentum k at temperatures 80, 160, 240, and 320 MeV.

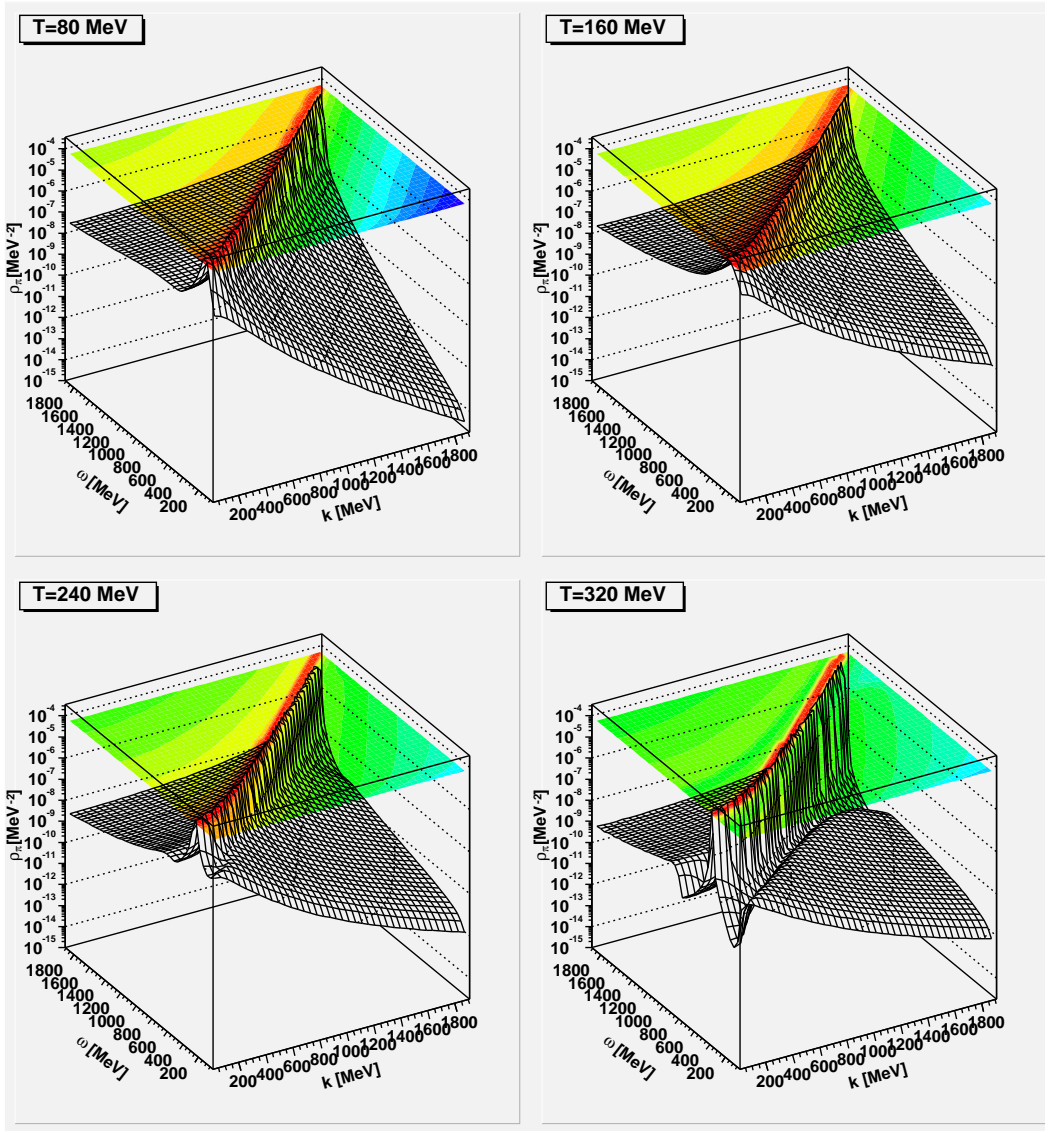


FIG. 7: The spectral density of the pion as a function of energy ω and momentum k at temperatures 80, 160, 240, and 320 MeV.

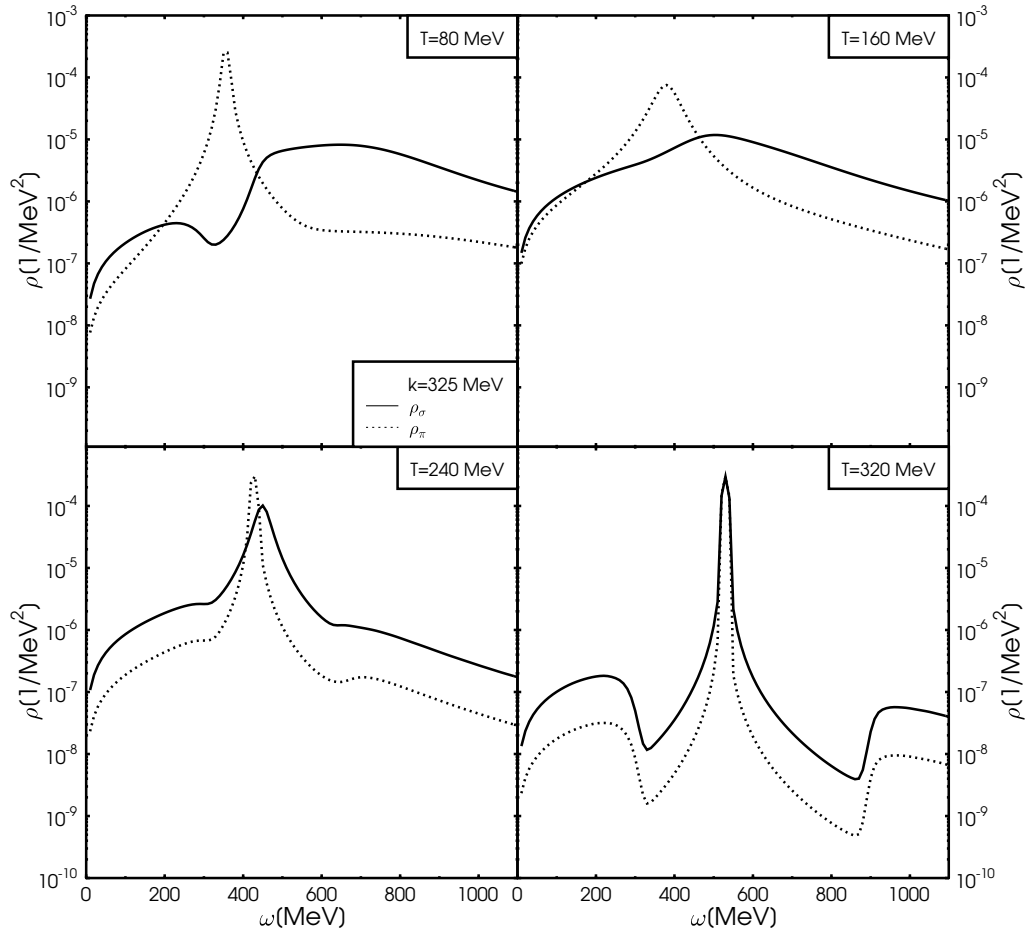


FIG. 8: The spectral density of the σ -meson and pion as a function of energy ω at temperatures 80, 160, 240, and 320 MeV. The momentum is $k = 325$ MeV.

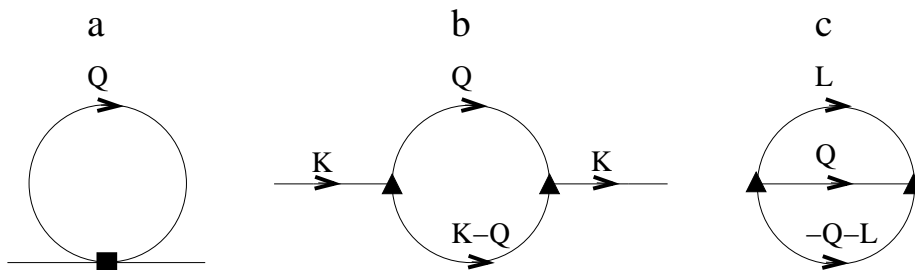


FIG. 9: The general topology of the tadpole diagram a, the cut sunset diagram b, and the sunset diagram c.